Journal of Molecular Graphics and Modelling 27 (2008) 266–274

Contents lists available at ScienceDirect

Journal of Molecular Graphics and Modelling

journal homepage: www.elsevier.com/locate/JMGM

Steered unfolding of ricin A and B chains

Debabani Ganguly, Chaitali Mukhopadhyay *

Department of Chemistry, University of Calcutta, 92 A.P.C. Road, Kolkata 700009, India

ARTICLE INFO

Article history:
Received 7 March 2008
Received in revised form 30 April 2008
Accepted 1 May 2008
Available online 4 May 2008

Keywords:
Mechanical unfolding
Pulling force
Ricin A-chain
Ricin B-chain
Steered molecular dynamics simulation

ABSTRACT

Highly toxic, heterodimeric protein ricin binds itself to the cell surface glycolipids or glycoproteins via its B-chain. The toxic A-chain halts protein synthesis by inactivating the ribosomes, leading to cell death. The translocation step requires partial unfolding of the protein. In this work mechanical unfolding of intact ricin as well as the individual A- and B-chains has been studied. A total of 110 ns simulation run has been performed to observe the unfolding of ricin dimer using steered molecular dynamics simulation. A gradual unfolding against a constant pulling velocity is observed for the ricin A-chain leaving the B-chain in its native-like structure. The breakage of the disulfide linkage connecting the two chains and reversal of the pulling ends of B-chain surprisingly reversed the picture as the B-chain starts to unfold from its N-terminal end. Due to the unfolding of B-chain from N-terminal end, the A-chain appears structurally rigid, which comes from the strong interfacial interactions (hydrophobic, hydrogen bonding, salt bridge). Mechanical unfolding of the individual monomers has also been performed to compare their stabilities in the monomeric and dimeric forms.

1. Introduction

A large number of plant and bacterial toxins of 'A–B' type have two different types of polypeptide chains one having enzymatic activity that resides in the A component [1] while the other (B-type chain) is responsible for binding of the toxin to the cell surface receptors. After binding to cell surface receptors via their B components, the toxins are endocytosed and finally get translocated into the cytosol [1–3]. Ricin is such a heterodimeric protein produced in the seeds of the castor oil plant (*Ricinus communis*). It is extremely toxic to mammalian cells. The A-chain is able to fatally disrupt protein synthesis by attacking the Achilles heel of the ribosome [4–6]. It has been reported that a single molecule of ricin reaching the cytosol can kill the cells as a consequence of the inhibition of protein synthesis. The ready availability, coupled with its extreme potency, has identified ricin as a potential biological warfare agent. The United States Center for Disease Control lists ricin as the second highest in the priority list as an agent for terrorism [7]. Therapeutically, the cytotoxicity of ricin has encouraged its use in 'magic bullets' to specifically target and destroy cancer cells, and the unusual intracellular trafficking properties of ricin potentially permit its development as a vaccine vector [6].

The cell entry by ricin is reported to involve a series of steps [6]. First, ricin binds itself to a range of cell surface glycolipids or glycoproteins having β-1,4-linked galactose residues via its B-chain (RTB). It then penetrates into the cell by endocytosis and the entry of the toxin into the cell is followed by a myriad of processes involving transport to Golgi complex and finally interfering with protein synthesis leading to cell death. The translocation step requires partial unfolding of the A-chain [8]. It is assumed that membrane traversal is preceded by unfolding of ricin A-chain, followed by refolding in the cytosol to generate the native, biologically active toxin. However, in the cytosol the structure of B-chain remains unaltered throughout the process.

Though there had been numerous studies on the mode of action of these types of toxins, the reason for such diverse functions of the two distinct chains as well as the difference in their zone of action is intriguing. Not only the structure, but also the relative stabilities of the two components might be crucial in these types of proteins. Also the importance of the interface in controlling the integrity of the dimeric form is not known. In case of ricin, the toxic action requires the dissociation of the heterodimer to its monomeric components. Also, the reduction of the disulfide bond connecting the A- and B-moieties of ricin is required for optimal enzymatic activity [9]. Understanding the dynamics of the dissociation of the ricin, the different mechanical stability of the two monomers as well as the role of the disulphide bond in the dissociation process are therefore critical for devising methods to block the action of

* Corresponding author. Tel.: +91 33 2350 8386; fax: +91 33 2351 9755.
E-mail addresses: chaitalicu@yahoo.com, cmchem@caluniv.ac.in (C. Mukhopadhyay).

Abbreviations: SMD, steered molecular dynamics; RTA, ricin A-chain; RTB, ricin B-chain; RMSD, root mean square deviation.

1093-3263/$ – see front matter © 2008 Elsevier Inc. All rights reserved.
doi:10.1016/j.jmgm.2008.05.001

Table 1
Description of the pulling path as well as the results of applying forces along the specific direction of the protein chain of different sets

Set	System pulled	Pulling direction	Time (ns)	Unfolding status
1 (1–5)	Dimer with disulphide bond	N-terminal of A and C-terminal of B	12.5, 10(×4)	A unfolds, B does not
1 (a)	Dimer without disulphide bond	N-terminal of A and C-terminal of B	10	A unfolds, B does not
2 (1–5)	Dimer without disulphide bond	N-terminal of A and N-terminal of B	12.5, 10(×4)	B unfolds faster
3	A-chain	N-terminal and C-terminal	10.5	Unfolds
4	B-chain	N-terminal and C-terminal	10	Unfolds

this lethal toxin. To provide molecular-level insights into the dynamics of ricin dissociation, we have used steered molecular dynamics (SMD) [10] simulation to mechanically unfold ricin under a constant pulling speed. The nature of unfolding of A and B-chains in the state of heterodimer (with and without the disulphide linkage between them) as well as in their free states have been investigated. We wanted (i) to see the effect of the disulphide linkage on the case of unfolding, (ii) to identify the differences in the unfolding dynamics of A- and B-chains, and (iii) to identify the differences in monomer and dimer unfolding.

2. Methods

SMD implemented in CHARMM (Version c31b1) [11] has been used to monitor the forced unfolding of the heterodimer as well as the individual chains of the ricin. The forces were applied to two atoms, which were selected as detailed in Table 1. In this numerical experiment we have pulled the chains along the terminals. For individual monomers (Sets 3 and 4) the system has been pulled along the two terminals for easy unfolding. For dimer, basically we wanted to pull the system along the two terminals of the system. The interface region consists of the C-terminal of chain A and N-terminal of chain B which must be very stable region. So initially to unfold the system the N-terminal of A-chain and C-terminal of B-chain have been pulled. As the results showed the appreciable unfolding of the A-chain, but not for the B-chain, we have pulled the B-chain along the other terminal. The close look in the structure of the dimer revealed that there was no space for the B-chain to be unfolded along the C-terminal end. We have also repeated the simulation experiment after removing the disulphide bond between the two monomers (Set 1b), however, B-chain did not unfold due to the same reason. In Set 2, after deleting the disulphide bond the B-chain has been pulled along the N-terminal and it was observed that the chain has started to unfold. According to CHARMM implementation, the forces applied on these two atoms are identical in magnitude, parallel to the vector connecting the two atoms, and in opposite directions in such way as to force an expansion rather than a compaction of the protein. During the simulations, the center of mass of the protein was kept fixed. A similar strategy using CHARMM has been used recently by Gao et al. [12].

The starting structure of ricin from *R. communis* was retrieved from X-ray crystal structure [13] (PDB code: 2AAI, 2.5 Å). CHARMM

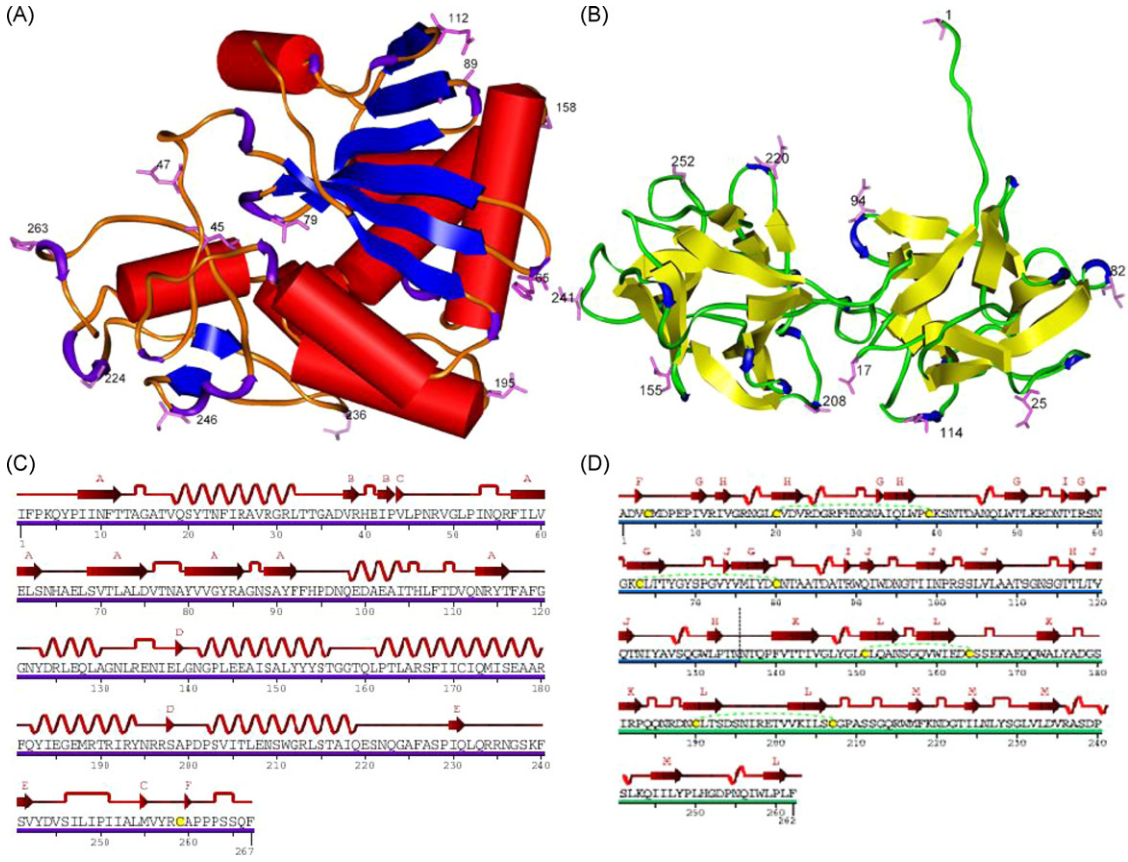

Fig. 1. Secondary structures of (A) ricin A-chain and (B) ricin B-chain. Sequence details of (C) A and (D) B-chain obtained from www.rcsb.org. The details of secondary structure of two chains have been provided by DSSP algorithm [28].

param22 all atom force field was used. Because of the large size (529 residues) of ricin, we have used implicit solvent model [14] using GBSW [15] approach in CHARMM to lower the computational cost. The protein structures were hydrogenated with HBUILD option of CHARMM. All the systems were energy minimized using ABNR (Adopted Basis Newton–Raphson) technique until the RMS gradient reached at 0.0001. Simulations were carried out with an integration time step of 1 fs, 14 Å cutoff for the non-bonded interactions and the coordinates were saved every 2 ps interval. To optimize the pulling speed and the force constant of the spring, the pulling speed was varied from 0.05 to 0.1 Å ps^{-1} and the force constant of the spring was varied from 2.5 to 2.8 N m^{-1}. No unfolding was observed at the lower values up to 4.5 ns simulation run. Thus, the pulling speed for the constant velocity stretching simulation was kept at 0.1 Å ps^{-1} and the force constant of the spring was maintained at 2.8 N m^{-1}. With these two combinations the appreciable starting of unfolding was achieved within 5 ns. The force constant of 2.8 N m^{-1} was also used by other group previously [16,17]. We observed practically no unfolding at lower pulling rate. The pull rate used in this work initiates the unfolding of ricin chain within an achievable time scale. The use of higher pulling velocity may lead to non-equilibrium effects, which may introduce obvious errors to the simulation results [18]. The lower pulling velocity may overcome all the artifacts, however, the corresponding computational cost will be very expensive.

Before starting SMD simulation, each system was heated gradually up to 300 K and then equilibrated for 150 ps. After equilibration the equilibrated structure has been used as the starting structure of the SMD simulation. The unfolding has been observed for a number of sets as described in Table 1. The heterodimer of ricin has a disulphide linkage between Cys259 of A-chain and Cys4 of B-chain. After breaking the inter-chain disulfide bond, the chains were pulled along the same directions as in Set 1a. The pulling direction of the B-chain has been altered to the main chain nitrogen of the N-terminal in Set 2. Sets 3 and 4 are the systems of the individual chains.

3. Results and discussion

It is well known that ricin binds to the cell membrane first through its B-chain and then A-chain gets translocated across the membrane. We wanted to compare the mechanical stability of the two chains as well as the effect of the inter-chain disulphide linkage on the stability of the dimer. SMD has been used recently to study the force-induced dimer dissociation of insulin [19], mechanical unfolding of protein [12,20–26]. Appreciable differences have been observed during the simulations of the five different sets of the protein system (Table 1). Fig. 1 shows the secondary structures of the two chains (1A and B) and their PDB structures (1C and D). Figs. S1–S4 in supplementary material show the residue wise plot of the change of secondary structure of the chains with respect to time.

3.1. Unfolding study of the dimer (Set 1)

The A- and B-chains of ricin are linked via a disulphide linkage between Cys259 of A- and Cys4 of B-chains. In Set 1 (with the S–S

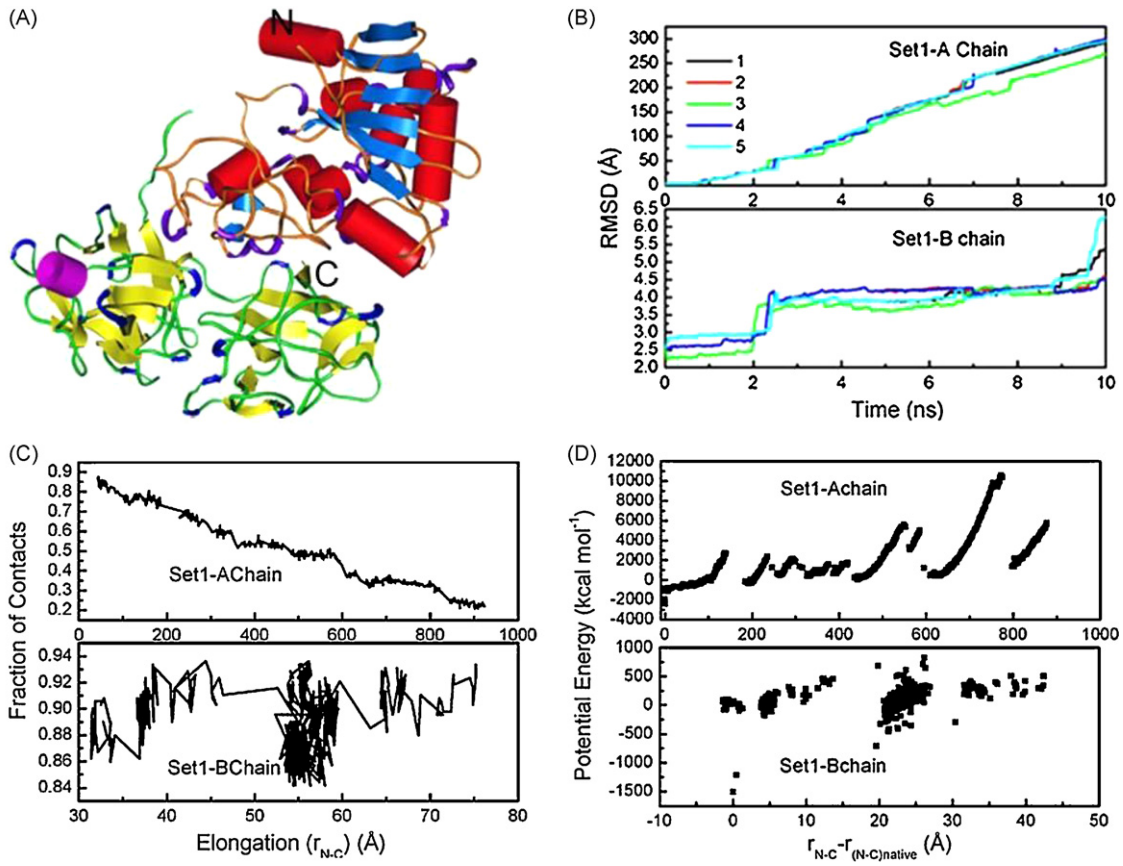

Fig. 2. Results of Set 1: (A) starting structure of Set 1, (B) backbone RMSD of individual chains (A and B) of ricin of five different trajectories is plotted as a function of simulation time. Data of only 10 ns time scale are shown, (C) fraction of contact as a function of elongation (r_{N-C}) of the individual chain is plotted for a single trajectory. The elongation of this particular set implies the distance between N-terminal of A-chain and C-terminal of B-chain. The results are calculated from the 10 ns time scale of a particular trajectory of the five and (D) For a single trajectory potential energy of each chain is plotted against $r_{N-C0} - (r_{N-C})_{native}$.

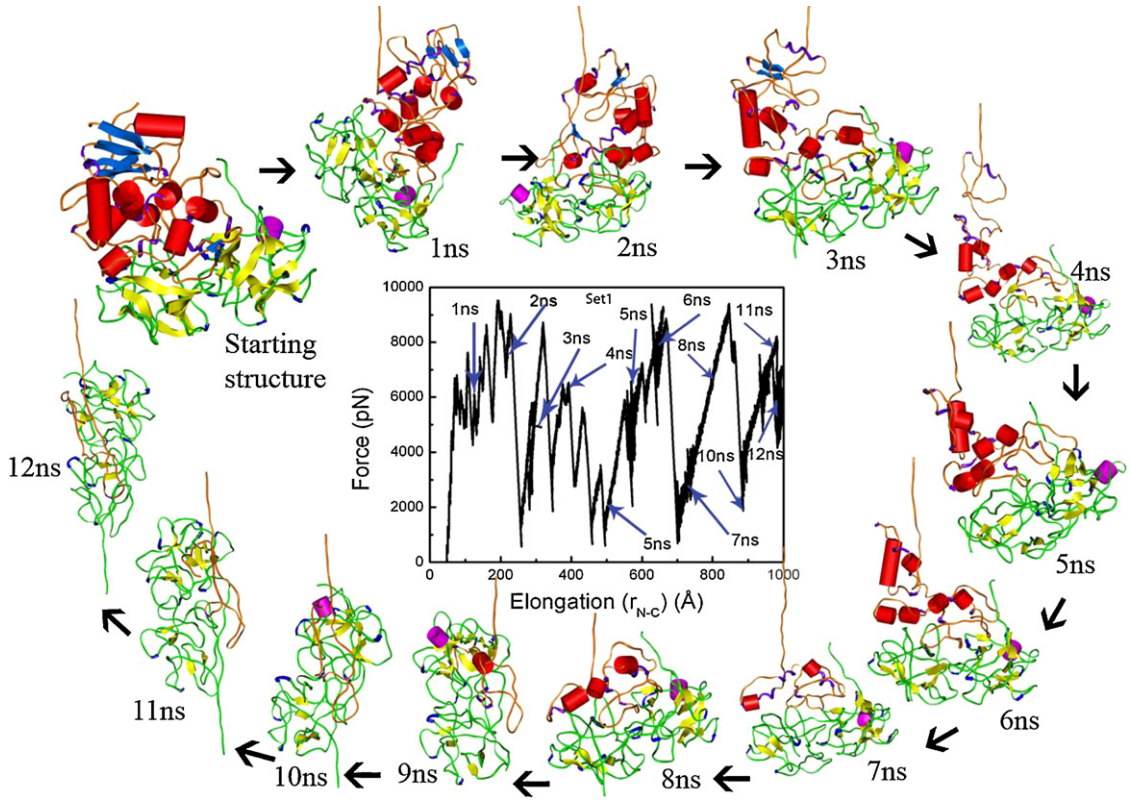

Fig. 3. The cyclic arrangement of the snapshots of Set 1 taken at 1 ns interval from 1 to 12 ns. Secondary structures of A- and B-chains are shown in different colour codes (A-chain: helix, red; sheet, blue; turn, violet; random coil, orange; B-chain: helix, pink; sheet, yellow; turn, blue; random coil, green). For simplicity the extended portion of the chain is truncated and the remaining portion of the protein chain is the main focus area. The plot of pulling force of the dimer (Set 1) as a function of reaction-coordinate, i.e. elongation (the elongation of this particular set implies the distance between N-terminal of A-chain and C-terminal of B-chain) is embedded in the center.

linkage intact) the dimer was pulled along the N-terminal of A and C-terminal of B-chain, respectively (Fig. 2A). Five independent trajectories were simulated for atleast 10 ns each. One of them was extended up to 12.5 ns. Fig. 2B shows the root mean square deviation (RMSD) of the backbone of the two chains of Set 1 from the crystal structure as a function of time. The similarity of the trajectories indicates that in all the runs the protein unfolds in a similar manner. It is evident that in Set 1, A-chain unfolds within 10 ns and reaches a nearly linear conformation. However, the structure of B-chain remains practically unaltered during this period. The B-chain is starting to unfold after 9.5 ns, however, the rate of unfolding is very slow. The timeline plots of the secondary structure, as given in supplementary materials, show the fate of pulling for every chain of each system. Fig. S1 (b) clearly shows that the B-chain unfolds very little within 12.5 ns time scale.

The compactness of the protein structure can be estimated quantitatively by calculating the change in the total number of the tertiary contacts with time. The tertiary contacts are counted if any atom of a side chain comes within 6 Å of another atom from a different side chain. The fraction of contacts as a function of N–C distance shows a gradual decrease in case of the A-chain where as that of chain B fluctuates around a N–C distance of 50–60 Å in Set 1 (Fig. 2C). This again indicates a gradual unfolding of A-chain upon pulling along its N-terminus, while B-chain shows an unusual stability towards pulling along its C-terminus. Similar observations have been reported earlier in the cases of insulin dimmer [19] and fibronectin [23] domains using SMD simulations.

We have defined the difference in the instantaneous N–C distance of the two chains from their native N–C distance as the reaction coordinate of the steered unfolding process. A plot of the potential energy of the individual chains as a function of the reaction coordinate is shown in Fig. 2D. It is seen from the plots that while the elongation of the A-chain is associated with a series of initial low energy barriers that of the B-chain is rather flat. The simulated force vs. elongation graph for the longest trajectory of Set 1 is shown in Fig. 3. The curve shows characteristic "saw tooth-shaped" major peaks with uneven spacing between the peaks. Since in this set the chain B remains practically native-like, the uneven spacing between peaks indicate differences in the ease of unfolding of different parts of the A-chain. Fig. 3 also shows the snapshots of the dimer taken from the 12.5 ns trajectory at 1 ns time interval. One can see from the individual snapshots that A-chain unfolds along the time, whereas the chain B unfolds very slowly within 12 ns, though it starts to unfold after 9.5 ns as seen from the backbone RMSD (Fig. 2B). The positions of different snapshots are marked in the force-elongation curve. Although the snapshots are equally spaced in time, the nature of the curve joining them or even the separation between them along the elongation pathway is quite different. This indicates that the individual secondary structural elements and the contacts holding them have different mechanical stability.

Ricin A-chain contains three distinct domains [13] (Fig. 1A and C). The first domain comprises of residues 1–117 with a five β-stranded sheets, the second domain (residues 118–219) contains five helices, while the last domain (residues 220–267) contains β-sheets. The initial slope of the force vs. elongation plot of 18–26 N m^{-1} (in all the five trajectories) is required to open the first β-strand within 1 ns. The second major peak (2–6 N m^{-1}) is required to open the first 2α-helices. Considerably higher force is required (10–16 N m^{-1}) to open up the β sheets. The C-terminal helices require a slope of 4–7.5 N m^{-1} to open up. This indicates that the regions of the polypeptide chain in β structures are more

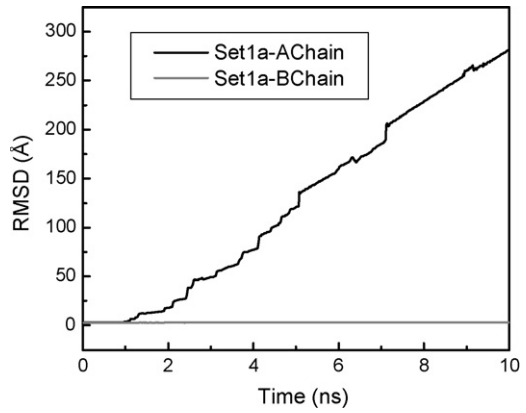

Fig. 4. Plot of backbone RMSD of A- and B-chain for Set 1a as a function of time where the dimer without the disulphide bond has been pulled along the N-terminal of A and C-terminal of B-chain for 10 ns time scale.

mechanically stable than helices, which has been also reported earlier for other proteins [27].

3.2. Unfolding of the dimer without the S–S linkage (Set 2)

In order to understand the role of the inter-chain disulphide linkage on the unfolding of the ricin chains we have simulated the dimer after removing the S–S bond. The dimer was pulled along the main chain nitrogen of the N-terminal of A-chain and the main chain carbon of the C-terminal of B-chain with a constant velocity. However, with this pulling direction the situation remained the same as in Set 1 (Fig. 4), i.e., the B-chain remain folded and the A-chain opens up gradually (Set 1a in Table 1). This indicates that whether or not the S–S bond is broken, pulling along the main chain carbon of the C-terminal of B will leave it practically native-like, while A can be opened up as in Set 1.

On the contrary, this situation drastically changes when the main chain nitrogen atom of the N termini of both the chains were pulled (Set 2) (Fig. 5A). Under this situation the nature of unfolding of the two chains gets significantly altered. The Fig. 5B shows the backbone RMSD of the individual chains from the crystal structure as a function of time. It is evident from the figure that the B-chain opens up upon the rupture of the disulphide bond provided it is pulled along the N terminus. However, the progress of unfolding of A is considerably different in this situation. In three trajectories out of five, the maximum RMSD reached was 110 Å, while in Set 1 it was nearly 300 Å. This indicates an incomplete unfolding of A-chain. The fraction of contact vs. N–C distance plot for Set 2 (Fig. 5C) also shows that for A-chain the unfolding is not complete, while B-chain reaches an elongation of 600 Å (compared to 75 Å in Set 1). The potential energy plot (Fig. 5D) along the reaction coordinate for these two polypeptide chains is quite different from that of the Set 1. The potential energy of the individual chains were calculated and plotted along the reaction coordinate. For B-chain, initial low energy barriers are followed by two high energy barriers (Fig. 5D). Though B-chain has been elongated to a much larger extent compared to the Set 1, at the end of 12 ns trajectory 50% of

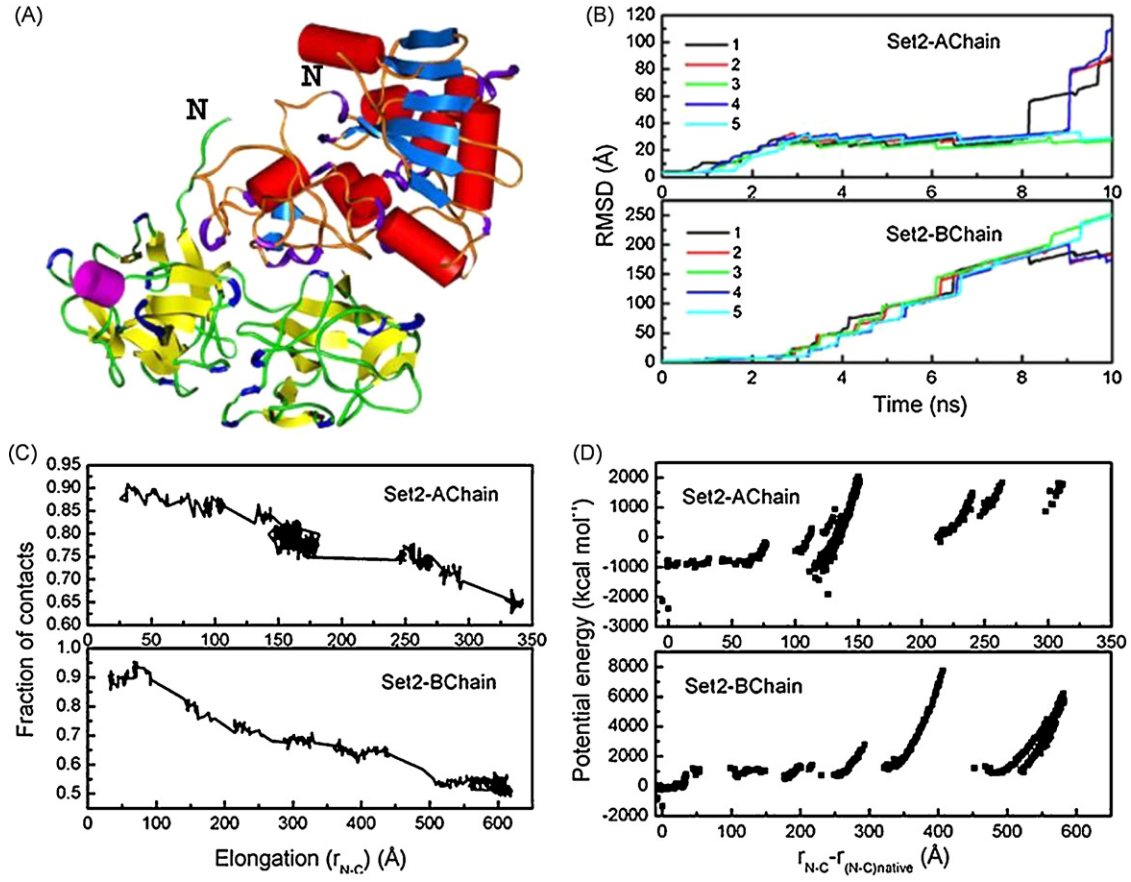

Fig. 5. Results of Set 2: (A) starting structure of Set 2, (B) backbone RMSD of individual chains (A and B) of ricin of five different trajectories is plotted as a function of simulation time. Data of only 10 ns time scale are shown, (C) fraction of contact as a function of elongation (r_{N-C}) of the individual chain is plotted for a single trajectory. The elongation of this particular set implies the distance between N-terminal of A-chain and C-terminal of B-chain. The results calculated from the 10 ns time scale of a particular trajectory of the five and (D) for a single trajectory potential energy of each chain is plotted against $r_{N-C} - (r_{N-C})_{native}$.

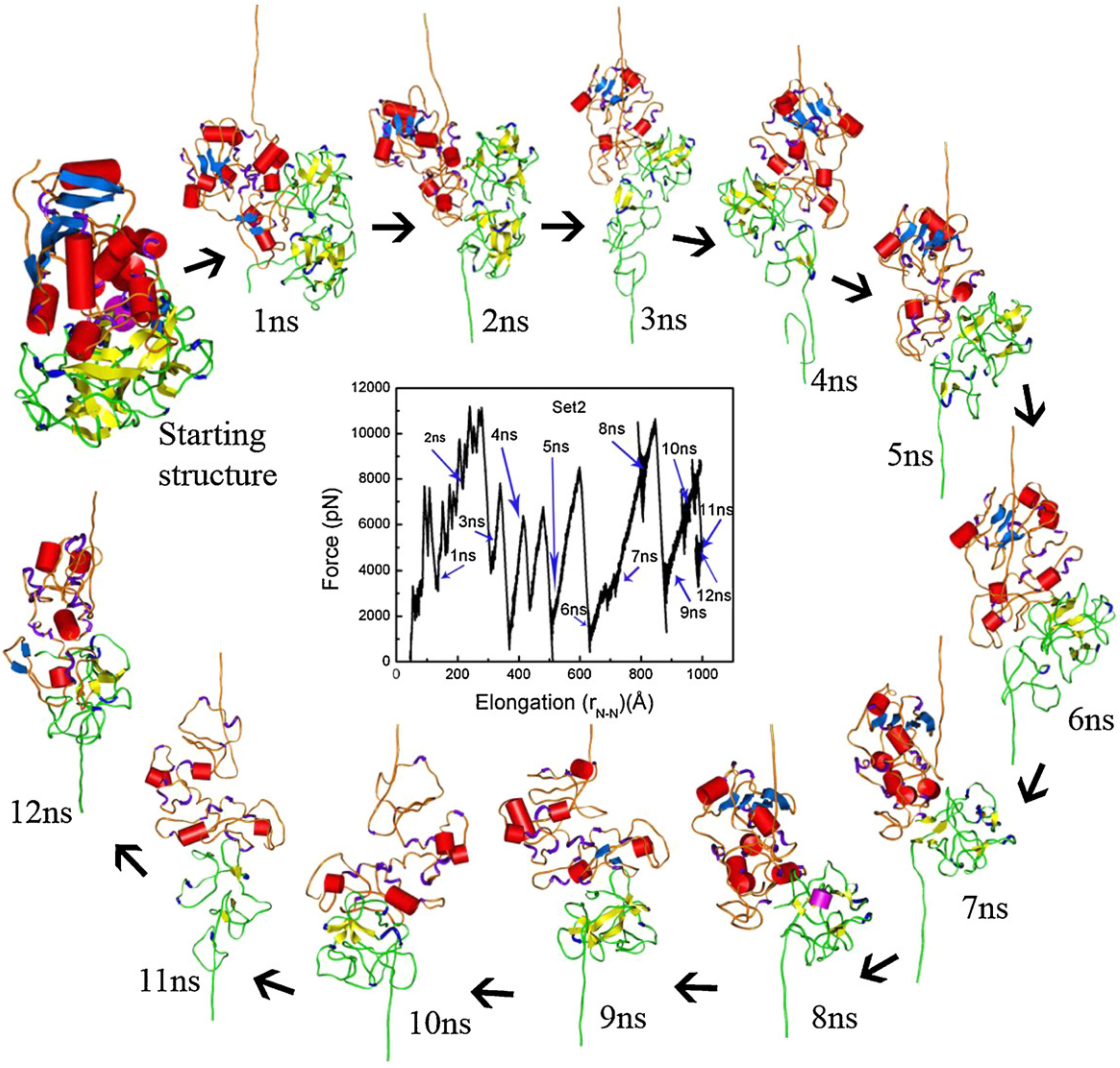

Fig. 6. The cyclic arrangement of the snapshots of Set 2 taken at 1 ns interval from 1 to 12 ns. Secondary structures of A and B-chains are shown in different colour codes (A-chain: helix, red; sheet, blue; turn, violet; random coil, orange; B-chain: helix, pink; sheet, yellow; turn, blue; random coil, green). For simplicity the extended portion of the chain is truncated and the remaining portion of the protein chain is the main focus area. The plot of pulling force of the dimer (Set 2) as a function of reaction coordinate, i.e. elongation (the elongation of this particular set implies the distance between N-terminal of A-chain and C-terminal of B-chain) is embedded in the center.

contacts still remains (Fig. 5C). The force vs. elongation plot (Fig. 6) is difficult to interpret in this case as this involves unfolding of both the chains. The 1 ns spaced snapshots are shown in Fig. 6. It is seen from the figure that unlike Set 1, the C-terminal helices of the A-chain are retained in Set 2. Ricin B-chain contains two identical domains (Fig. 1B and D). It is seen that the C-terminal domain is retained, while the N-terminal domain opens up.

It is interesting to note that the unfolding behaviour of the two chains of ricin is dependent not only on the pulling direction, but also on the existence of the intact A–B interface. Fig. 7 shows the interface of the A- and B-chains of ricin. There are few hydrogen bonds and hydrophobic contacts present at the interface [9]. In particular, the C-terminal residue Phe262 of B-chain is linked to Arg235 of A-chain by a salt bridge and is hydrogen bonded to Tyr183 of A-chain. This makes the C-terminal residue of B-chain very secure and prevents the C-terminal end of the B-chain from opening up in the dimeric form. On the other hand, there are several residues of the C-terminal of A which are directly forming contacts with the B-chain. The unfolding of A-chain thus depends on the presence of the intact A–B interface and the compactness of B-chain. This feature of unfolding of the two chains was consistent in all the five independent trajectories of Sets 1 and 2.

3.3. Individual chains: A and B (Sets 3 and 4)

The mechanical unfolding of A- and B-chains of ricin were investigated separately. In Set 3 the nature of unfolding of the A-chain resembles closely to that observed for the A-chain in the intact dimeric form (Set 1). This is indicated in the plots of backbone RMSD from the crystal structure and fraction of contacts (Fig. 8A and D). It is clearly seen that the A-chain extends upto 1000 Å within 10 ns and looses nearly 90% of the contacts (Fig. 8D). The potential energy vs. reaction coordinate plot (Fig. 8E) also shows several low to moderate energy barriers. The peak heights are lower compared to that of the dimer (Fig. 2D).

The Set 4 contains the data for unfolding of B-chain in the monomeric form. B-chain is a lectin and has two distinct domains. The domain 1 contains amino acids ranging from (1–135) with 13 β sheets and domain 2 (136–262) has 12 β sheets. The structure of B-chain is rigid towards a mechanical pull along C-terminal when it is in dimeric form, but the compactness of the structure decreases in the free form. As discussed earlier this might be due to the presence of salt-bridge/hydrogen bonds and hydrophobic interactions between the interfacial regions. Thus, when individual monomers are treated with the same pulling speed, they behave

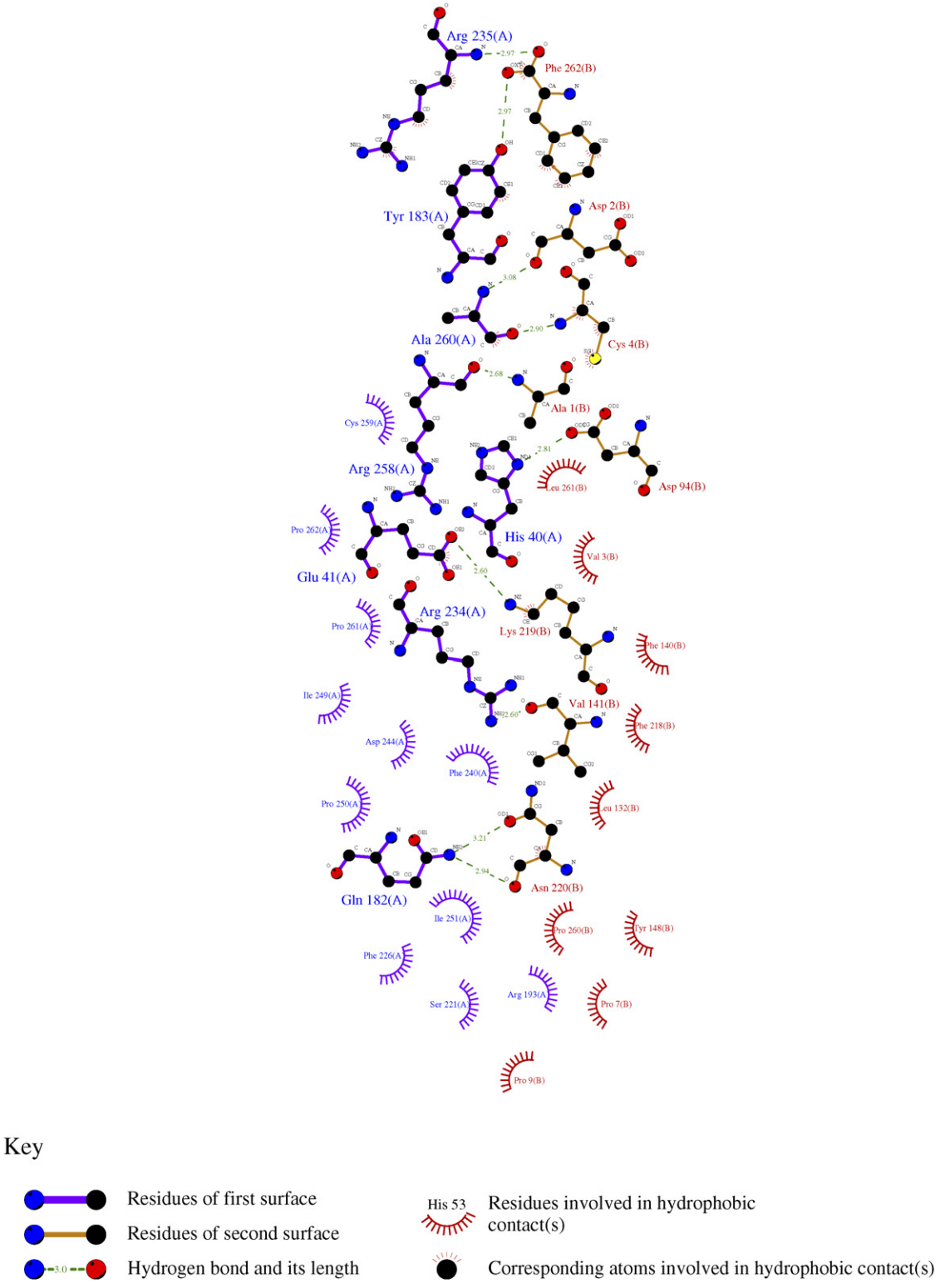

Fig. 7. Dimeric interface of A- and B-chains plotted with LIGPLOT [29].

differently. In Set 4, backbone RMSD of B-chain from the crystal structure and the change of fraction of contact (Fig. 8B and D) shows that the unfolding is more complete in the monomeric form. Fig. 8B also contains the plots of backbone RMSD of different regions of B-chain as a function of time. It can be seen that regions of 22–45 and 237–260 show unusual stability. These two regions are the sugar binding sites of B-chain. The B-chain starts to unfold from the C-terminal end, which is different from that observed in Set 2, leaving the N-terminal folded. For Set 4, the first peak in the force vs. elongation curve (Fig. 8C) (at 137.9 Å) appears due to the opening of the first two C-terminal β strands with slope of 9 N m^{-1} around 1.2 ns in the force vs. elongation plot. At this time the N-terminal β sheet also starts to open up. The next four β strands of domain 2 open (272 Å) with a slope of 14.9 N m^{-1} within 2.7 ns.

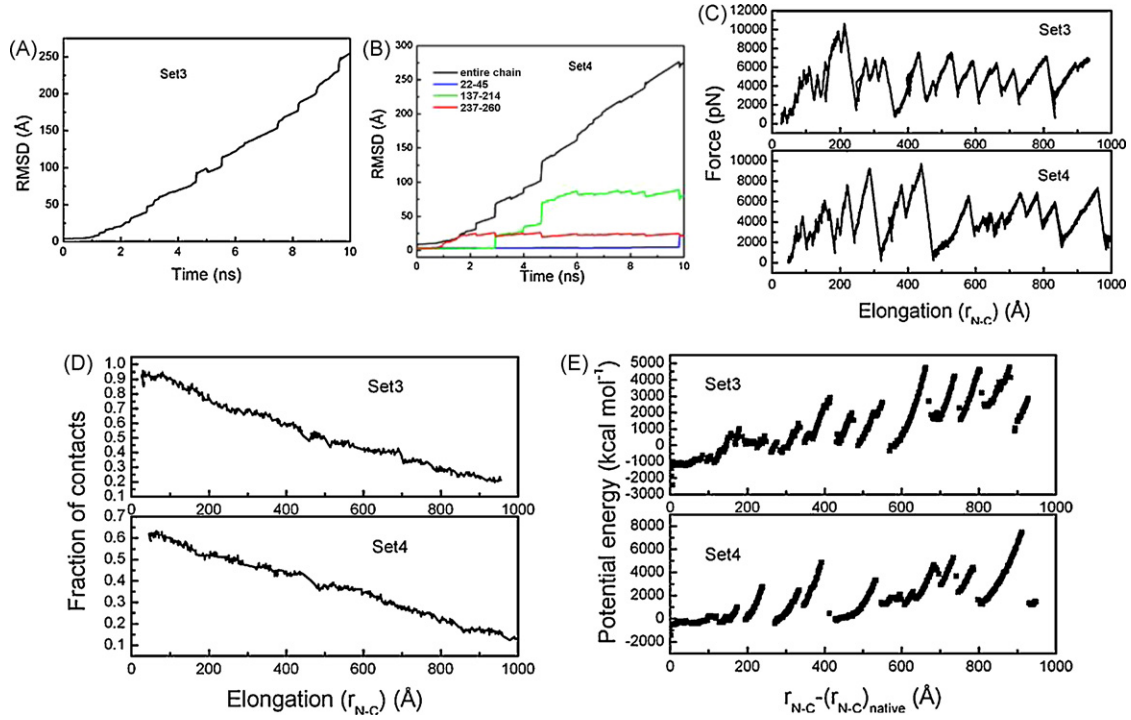

Fig. 8. Results of individual monomers, Sets 3 and 4: backbone RMSD of (A) A-chain (Set 3) and (B) B-chain as a function of time (Set 4) for 10 ns time scale, (C) Pulling force of A- and B-chain as a function of elongation, i.e. N–C distance, (D) Fraction of contact as a function of elongation (r_{N-C}) of the individual chain, and (E) Potential energy of each chain is plotted against $r_{N-C} - (r_{N-C})_{native}$.

The third peak of 5 N m^{-1} appears at 4.4 ns after complete opening of the domain 2 (up to 422.56 Å). The last significant peak of the curve appears at 9.6 ns with a slope of 5 N m^{-1} where two β strands and the joining turn are unfolded (upto 941 Å). The fraction of side chain contacts of the chains are plotted in Fig. 8D as a function of N–C distance. No intermediate state was observed from the plots as observed in case of Sets 1 and 2.

It is found from the above-mentioned results of the SMD simulation that the absence of the disulfide bond between the two monomers highly altered the unfolding dynamics of the ricin. In Set 1, A-chain readily unfolds without formation of any significant intermediate states. However, the B-chain, when pulled along the C-terminal, behaves as a highly rigid structure. Total 12.5 ns simulation with a constant pulling speed results only ∼75 Å elongation of the chain length. Change of pulling direction of the B-chain (N-terminal) does not improve the condition. Surprisingly in Set 2 after deletion of the disulfide bond and pulling along the N-terminal, the B-chain starts to unfold and after 12.5 ns the N–C distance of the B-chain reaches at ∼600 Å. Surprisingly, the "rate" of unfolding of A-chain becomes significantly low compare to that of Set 1 and the unfolding was incomplete even after 12.5 ns. Several C-terminal helices of A did not open under this situation, where as in Set 1, where the B-chain was practically unfolded, the A-chain opened up rather smoothly.

This can be explained by considering the residues involved at the A–B interface (Fig. 7). As shown in Fig. 7, there are number of hydrogen bonds, salt bridges and the hydrophobic interactions present in the interfacial region of the dimer. This inter-domain interactions probably the cause of the structural rigidity of the two chains. The absence of these inter-domain interactions causes the easy unfolding of the individual monomers when they are treated with the same pulling speed.

There are several residues of the C-terminus of the A-chain that participate in the interface formation. The Tyr183 and Arg235 of A-chain are involved in hydrogen bonding and salt bridge interaction with the C-terminal residue Phe262 of B-chain. In addition, Gln182, Asn220, Ile251 and Phe226 are also involved in either hydrogen bonding or hydrophobic contact with the C-terminal residues of the B-chain. In Set 1, while B-chain is pulled along the C-terminal these contacts are broken, leading to weakening of the A–B interface. This allowed the C-terminal helices of the A-chain to open up under the pulling force in Set 1. It is also seen in Fig. 2D that the opening up of the C-terminal helices of the A-chain is associated with a larger energy cost.

However, in Set 2 while pulling along the N-terminus of B-chain, the contacts between the C-termini of the two chains remain intact. This prevents the C-terminal helices of the A-chain from unfolding. Mechanical unfolding of the individual monomer under the same condition shows that both the chains could be elongated up to a length of ∼900 Å (Fig. 8C), though the two binding sites of the B-chain retain considerable secondary structures (Fig. 8B). The change of secondary structures with respect to time (Figs. S1–S4) and the radius of gyration as a function of time (Figs. S5–S7) of dimer and monomers are given in supplementary materials. Fig. S8 shows the change of number of hydrogen bonds with time for Sets 1 and 2.

It is well known that the cellular entry by the protein toxins (e.g., diphtheria, Shiga, cholera, etc.) involves the same generalized mechanism [8], which includes the initial binding of the non-enzymatic part to the cell surface, followed by endocytosis. After the endocytic uptake, in order to reach the ribosomal substrates, the ricin A-chain must cross the luminal membrane. It is assumed that the membrane traversal is preceded by unfolding of ricin A-chain [8]. From the observed differences of the unfolding pattern of the dimer under different pulling conditions, we hypothesize the following mechanism of ricin action. First the B-chain adheres to the membrane. The N-terminal part of the A-chain can then be unfolded to facilitate the translocation. In the second stage the S–S

bond breakage and the loss of contacts between the C-termini of the two chains will ensure complete unfolding of the A-chain. Since the two binding sites of the B-chain are mechanically more stable than the rest of the chain, it is likely that B-chain will be dislodged last from the membrane surface.

Acknowledgment

D.G. is thankful to CSIR for the financial support through CSIR-NET fellowship (sanction number: (9/28(575)/2002 EMR-I dated. 10.10.2002).

Appendix A. Supplementary data

Supplementary data associated with this article can be found, in the online version, at doi:10.1016/j.jmgm.2008.05.001.

References

[1] P.O. Falnes, K. Sandvig, Penetration of protein toxins into cells, Curr. Opin. Cell Biol. 12 (2000) 407–413.
[2] K. Sandvig, B. van Deurs, Entry of ricin and Shiga toxin into cells: molecular mechanisms and medical perspectives, EMBO J. 19 (2000) 5943–5950.
[3] K. Sandvig, B. van Deurs, Delivery into cells: lessons learned from plant and bacterial toxins, Gene Ther. 12 (2005) 865–872.
[4] S. Olsnes, A. Pihl, Ricin—a potent inhibitor of protein synthesis, FEBS Lett. 20 (1972) 327–329.
[5] S. Olsnes, R. Heiberg, A. Pihl, Inactivation of eucaryotic ribosomes by the toxic plant proteins abrin and ricin, Mol. Biol. Rep. 1 (1973) 15–20.
[6] M.J. Lord, N.A. Jolliffe, C.J. Marsden, C.S.C. Pateman, D.C. Smith, R.A. Spooner, P.D. Watson, L.M. Roberts, Ricin: mechanisms of cytotoxicity, Toxicol. Rev. 22 (2003) 53–64.
[7] L.G. Doan, Ricin: mechanism of toxicity, clinical manifestations, and vaccine development. A review, J. Toxicol. Clin. Toxicol. 42 (2004) 201–208.
[8] R.H. Argent, A.M. Parrott, P.J. Day, L.M. Roberts, P.G. Stockley, J.M. Lord, S.E. Radford, Ribosome-mediated folding of partially unfolded ricin A-chain, J. Biol. Chem. 275 (2000) 9263–9269.
[9] K. Sandvig, B. van Deurs, Endocytosis, intracellular transport, and cytotoxic action of Shiga toxin and ricin, Physiol. Rev. 76 (1996) 949–966.
[10] S. Izrailev, S. Stepaniants, B. Isralewitz, D. Kosztin, H. Lu, F. Molnar, W. Wriggers, K. Schulten, in: P. Deuflhard, J. Hermans, B. Leimkuhler, A.E. Mark, S. Reich, R.D. Skeel (Eds.), Computational Molecular Dynamics: Challenges, Methods, Ideas, Volume 4 of Lecture Notes in Computational Science and Engineering, Springer-Verlag, Berlin, 1998, pp. 39–65.
[11] B.R. Brooks, R.E. Bruccoleri, B.D. Olafson, D.J. States, S. Swaminathan, M. Karplus, CHARMM: a program for macromolecular energy, minimization, and dynamics calculations, J. Comput. Chem. 4 (1983) 187–217.
[12] M. Gao, D. Craig, O. Lequin, I.D. Campbell, V. Vogel, K. Schulten, Structure and functional significance of mechanically unfolded fibronectin type III_1 intermediates, Proc. Natl. Acad. Sci. 100 (2003) 14784–14789.
[13] W. Monfort, J.E. Villafranca, A.F. Monzingo, S.R. Ernst, B. Katzin, E. Rutenber, N.H. Xuong, R. Hamlin, J.D. Robertus, The three-dimensional structure of ricin at 28A, J. Biol. Chem. 262 (1987) 5398–5403.
[14] R. Roux, T. Simonson, Implicit solvent models, Biophys. Chem. 78 (1999) 1–20.
[15] W. Im, M.S. Lee, C.L. Brooks III, Genaralized born model with a simple smoothing function, J. Comput. Chem. 24 (2003) 1691–1702.
[16] H. Grubmüller, B. Heymann, P. Tavan, Ligand binding: molecular mechanics calculation of the streptavidin–biotin rupture force, Science 271 (1996) 997–999.
[17] Y. Xu, J. Shen, X. Luo, I. Silman, J.L. Sussman, K. Chen, H. Jiang, How does Huperzine A enter and leave the binding gorge of acetylcholinesterase? Steered molecular dynamics simulations, J. Am. Chem. Soc. 125 (2003) 11340–11349.
[18] B. Isralewitz, M. Gao, K. Schulten, Steered molecular dynamics and mechanical functions of proteins, Curr. Opin. Struct. Biol. 11 (2001) 224–230.
[19] T. Kim, A. Rhee, C.M. Yip, Force-induced insulin dimer dissociation: a molecular dynamics study, J. Am. Chem. Soc. 128 (2006) 5330–5331.
[20] H. Lu, B. Isralewitz, A. Krammer, V. Vogel, K. Schulten, Unfolding of titin immunoglobulin domains by steered molecular dynamics simulation, Biophys. J. 75 (1998) 662–671.
[21] A. Krammer, H. Lu, B. Isralewitz, K. Schulten, V. Vogel, Forced unfolding of the fibronectin type III module reveals a tensile molecular recognition switch, Proc. Natl. Acad. Sci. 96 (1999) 1351–1356.
[22] P.E. Marszalek, H. Lu, H. Li, M. Carrion-Vazquez, A.F. Oberhauser, K. Schulten, J.M. Fernandez, Mechanical unfolding intermediates in titin modules, Nature 402 (1999) 100–103.
[23] E. Paci, M. Karplus, Forced unfolding of fibronectin type 3 modules: an analysis by biased molecular dynamics simulations, J. Mol. Biol. 288 (1999) 441–459.
[24] H. Lu, K. Schulten, Steered molecular dynamics simulations of force-induced protein domain unfolding, Proteins: Struct. Func. Genet. 35 (1999) 453–463.
[25] S.B. Fowler, R.B. Best, J.L.T. Herrera, T.J. Rutherford, A. Steward, E. Paci, M. Karplus, J. Clarke, Mechanical unfolding of a titin Ig domain: structure of unfolding intermediate revealed by combining AFM, molecular dynamics simulations NMR and protein engineering, J. Mol. Biol. 322 (2002) 841–849.
[26] S.P. Ng, R.W.S. Rounsevell, A. Steward, C.D. Geierhaas, P.M. Williams, E. Paci, J. Clarke, Mechanical unfolding of TNfn3: the unfolding pathway of a fnIII domain probed by protein engineering AFM and MD simulation, J. Mol. Biol. 350 (2005) 776–789.
[27] M. Sotomayor, K. Schulten, Single molecule experiments in vitro and in silico, Science 316 (2007) 1144–1148.
[28] W. KK Kabsch, C. Sander, Dictionary of protein secondary structure: pattern recognition of hydrogen-bonded and geometrical features, Biopolymers 22 (1983) 2577–2637.
[29] A.C. Wallace, R.A. Laskowski, J.M. Thornton, LIGPLOT: a program to generate schematic diagrams of protein–ligand interactions, Prot. Eng. 8 (1995) 127–134.